Improving PEMFC Performance Using Short-Side-Chain Low-Equivalent-Weight PFSA Ionomer in the Cathode Catalyst Layer

Improving PEMFC Performance Using Short-Side-Chain Low-Equivalent-Weight PFSA Ionomer in the Cathode Catalyst Layer

Yannick Garsany,[1,*,z] Robert W. Atkinson III,[2] Megan B. Sassin,[3] Rachel M. E. Hjelm,[4] Benjamin D. Gould,[3,*] and Karen E. Swider-Lyons[3,*]

[1]*EXCET INC., Springfield, Virginia 22151, USA*
[2]*ASEE Postdoctoral Program, US Naval Research Laboratory, Washington, DC 20375, USA*
[3]*US Naval Research Laboratory, Washington, DC 20375, USA*
[4]*NRC Postdoctoral Program, US Naval Research Laboratory, Washington, DC 20375, USA*

Incorporation of short-side chain (SSC) ionomers in the catalyst layers (CL) of proton exchange membrane fuel cells (PEMFCs) can improve performance, particularly at low relative humidities. We attempt to understand this effect by comparing PEMFCs with cathode CLs containing Pt on carbon-black (CB) and either SSC Aquivion ionomer or a standard long-side-chain (LSC) Nafion ionomer at 50% and 100% RH. The CL microstructures are characterized for their micro- and mesoporosity. The CLs are formed into PEMFCs and probed with polarization curves, cyclic voltammetry, O_2 gain, limiting current measurements, and electrochemical impedance spectroscopy. PEMFCs containing the SSC ionomer in the cathode CL have superior polarization curves compared to those containing the LSC ionomer in the mass transport region under all conditions. We find that the SSC ionomer imparts lower proton transport resistances, lower charge transfer resistance to the cathode near 0.60 V, and lower mass transport resistance at 0.40 V. We attribute some of the performance improvements to the superior proton conductivity of the SSC ionomer, and the remainder to the higher micropore volume in the SSC-containing CLs which can more effectively evaporate water to the gas phase, improving both the availability of catalyst sites for charge transfer and mesopores for gas transport.
 [DOI: 10.1149/2.1361805jes]

Manuscript submitted January 9, 2018; revised manuscript received March 30, 2018. Published April 13, 2018.

Proton exchange membrane fuel cells (PEMFCs) are clean and efficient electrochemical power sources for use in materials handling and transportation applications.[1] At the heart of the PEMFC is a membrane electrode assembly (MEA) comprising catalyst layers (CLs), a proton exchange membrane (PEM), and gas diffusion media (GDM). The micrometers-thick anode and cathode CLs on opposing sides of the PEM (i.e. Nafion) together form the catalyst coated membrane (CCM). The CL structure contains a continuous network of ionomer (i.e. Nafion) and electrocatalyst (i.e. carbon-black (CB) supported Pt catalyst (Pt/CB)) in contact with the PEM to promote proton transport between the PEM and catalyst. The carbon support typically contains micropores and the CL must also contain a percolating network of mesopores through the carbon/ionomer backbone to facilitate transport of gases to the catalyst and expulsion of product water from the CL.

The optimization of the CLs is essential for high fuel cell performance, particularly the cathode CL where the oxygen reduction reaction (ORR) takes place.[2–4]

$$O_2 + 4H^+ + 4e^- \rightarrow 2H_2O \quad [1]$$

In addition to having an active electrocatalyst for good kinetics, the electrodes must have the appropriate porosity and ionomer coverage for effective proton (H^+), gas, and water transport for operation at high current density.

The pore structures must provide ample pathways for O_2 to reach the cathode, plus allow clearing of the water generated by the fuel cell reaction, as any residual liquid water can flood the electrodes and block mass transport. A modeling study performed by Eikerling[5] has shown that an agglomerated CL structure with a bimodal micropore size distribution is ideal to evaporate water and maximize mass transport of reactants, protons, and products through the mesopores. According to Wang et al.,[6] an idealized three-phase composite electrode would have hydrophobic micropores for good macroscopic reactant transport and water evaporation, whereas the mesopores should be hydrophilized in order to achieve good wettability and proton accessibility. Further, as described by Eikerling,[5] when employing a bimodal δ-distribution for the pore size distribution, the cathode CL could exist locally in three distinct states: a dry state, an optimal wetting state, and a fully flooded state. In the optimal wetting state, local capillary equilibrium between liquid and gas phase exists in the primary or micropores (3 to 10 nm), which favors large reaction and evaporation rates. With the micropores managing water evaporation, the secondary or mesopores (10 to 40 nm) are open for gaseous transport of reactants and products. This bimodal pore size distribution is instrumental in optimizing competing requirements of high catalyst utilization and high power densities.

The ionomer coverage is also discussed as a key criterion for high power performance, as it provides the protonic pathways needed for the ORR in Eq. 1. Some ascribe to a model in which the ideal ionomer is adequately dispersed to cover all the Pt nanoparticles on the carbon surface for maximum utilization, thick enough for good proton conductance, and thin enough for low-resistance gas transport.[7] Under practical cell operating conditions, when the ORR is drawing currents exceeding 1–2 A cm^{-2}, it is theorized that the ionomer distribution becomes more important because of resistances to the mass transport of H^+ and O_2 in the ionomer film. At very thin or thick ionomer films, the transport of either H^+ or O_2 becomes the performance-controlling step of the ORR, respectively,[8] which may manifest itself as a charge transfer resistance.[9] Traditionally, PEMFCs utilize long-side-chain (LSC), perfluorosulfonic acid (PFSA) ionomer (i.e. Nafion) and much has been reported on the structure-relationships of LSC Nafion CLs.[1]

Due to its higher degree of crystallinity and thermal resistance,[10,11] attention is being paid to short side chain (SSC) PFSA ionomers both as membranes[12,13] and as a proton-conducting media dispersed into the CL.[14–19] Lei et al.,[14] Peron et al.,[15] and Park et al.[16] described the use of these SSC ionomers in the cathode CLs. These authors observed larger current densities at elevated temperature (i.e. 95°C and 110°C) and under lower relative humidity (RH, i.e. 70% to 30% RH) for PEMFCs prepared using the SSC PFSA ionomer compared to PEMFCs prepared using the LSC Nafion PFSA ionomer. Park et al.[16] ascribed the improved PEMFC performance with SSC ionomers in the

*Electrochemical Society Member.
[z]E-mail: yannick.garsany.ctr.fr@nrl.navy.mil

Table I. Properties of the SSC Aquivion CCMs, LSC Nafion CCMs, and the commercial Gore CCM used in this work.

Prepared SSC Aquivion CCMs for PEMFC testing		
	Anode CL	Cathode CL
Catalyst	50 wt% Pt/CB (Ion Power Inc.)	50 wt% Pt/CB (Ion Power Inc.)
Ionomer	Nafion 1100 EW	Aquivion 830 EW
I/C ratio	0.95/1 (32 wt% dry)	0.95/1 (32 wt% dry)
Pt loading	0.31 mg_{Pt} cm^{-2}	0.31 mg_{Pt} cm^{-2}
PEM	25 μm Nafion HP	
Prepared LSC Nafion CCMs for PEMFC testing and N_2-sorption porosimetery		
	Anode CL	Cathode CL
Catalyst	50 wt% Pt/CB (Ion Power Inc.)	50 wt% Pt/CB (Ion Power Inc.)
Ionomer	Nafion 1100 EW	Nafion 1100 EW
I/C ratio	0.95/1 (32 wt% dry)	0.95/1 (32 wt% dry)
Pt loading	0.31 mg_{Pt} cm^{-2}	0.31 mg_{Pt} cm^{-2}
PEM	25 μm Nafion HP	
Primea MESGA CCM A510.4/M710.18/C510.4 (W.L. Gore & Associates)		
	Anode CL	Cathode CL
Pt loading	0.10 mg_{Pt} cm^{-2}	0.40 mg_{Pt} cm^{-2}
PEM	18 μm	
Prepared SSC Aquivion CCMs for N_2-sorption porosimetry		
	Anode CL	Cathode CL
Catalyst	50 wt% Pt/CB (Ion Power Inc.)	50 wt% Pt/CB (Ion Power Inc.)
Ionomer	Aquivion 830 EW (I/C = 0.95/1))	Aquivion 830 EW (I/C = 0.95/1)
Pt loading	0.31 mg_{Pt} cm^{-2}	0.31 mg_{Pt} cm^{-2}
PEM	25 μm Nafion HP	

cathode CLs to the higher proton conductivity of the SSC ionomers and more effective trapping of water that is produced during the ORR compared to the LSC ionomer. Using scanning transmission electron microscopy (STEM), the authors also found that the SSC ionomer showed better continuity and uniformity on Pt and carbon particles than the LSC Nafion ionomer, which might have led to improvement of both mass transport and the proton conducting network in the CLs. However, there is dispute about the validity of using electron microscopy for evaluating ionomer coverage, due to the risk of beam damage from the electron source.[20]

The cell performances reported in the literature for PEMFCs containing SSC ionomer in their cathode CLs are less compelling when operating the fuel cell at 80°C in air, 100% RH and ambient pressure, and most literature reports no improvement or poorer performance from CLs with SSC ionomers at 100% RH.[14–16] At 100% RH, Park et al.[16] reported cell performance for their PEMFC utilizing SSC-1.02 ionomer (i.e. Aquivion 980 EW, 1.02 IEC) to be identical to that of their baseline PEMFC utilizing the LSC-0.99 ionomer (i.e. Nafion 1000 EW, 0.99 IEC). Their PEMFCs utilizing the SSC-1.43 ionomer (i.e. Aquivion 700 EW, 1.43 IEC) and SSC-1.83 ionomer (i.e. Asahi Kasei-Materials, 557 EW, 1.83 IEC) exhibit lower cell performances with larger polarization losses in the low current density region of 100–600 mA cm^{-2}.

We attempt to compare traditional LSC (i.e. Nafion-based) perfluorosulfonic acid ionomers in the cathode CLs to SSC Aquivion ionomers through non-microscopic techniques, and study the performance under RH of 50 and 100%. In addition to standard fuel cell polarization curves, we use N_2 porosimetry to examine the porosity distribution in the CL that is critical to water management and mass transport, and electrochemical impedance spectroscopy (EIS) to discern the contributions of charge transfer vs. mass transport limitations to the fuel cells and to compare the cathode proton transport resistance. We use limiting current measurements to determine the total O_2 transport resistance as a function of total pressure.

Experimental

Preparation of catalyst inks and fabrication of catalyst coated membranes (CCMs).—We briefly describe our ink formulations - all of the anode CLs were prepared with carbon-black supported Pt catalyst (Pt/CB, Ion Power (IP), 50 wt% Pt, information about manufacturer was not disclosed), and aqueous LSC Nafion ionomer solution in the proton form (Liquion solution LQ-1115, 1100 EW, 15 wt%, IP). All the cathode CLs were prepared using the same 50 wt% Pt/CB catalyst. The ionomeric binder in the cathode CL was either an aqueous SSC Aquivion ionomer from a solution in the proton form (Aquivion D83-06A, 830 EW, 6 wt%) or the conventional LSC Nafion ionomer that was also used in the anode CL.

The Pt catalyst inks for ultrasonic spray deposition were prepared by mixing the 50 wt% Pt/CB catalyst, Nafion or Aquivion ionomer solution, isopropyl alcohol, and pure water. The mass ratio of the ionomer binder to carbon black (I/C) was adjusted to 0.95/1 for both anode and cathode CL (i.e. 32 wt% ionomer in the dry CL). Nafion HP membranes (25 μm thick) were used as received. An automated ultrasonic spray coater was employed to deposit the anode CL (0.31 mg_{Pt} cm^{-2}) and the cathode CL (0.31 mg_{Pt} cm^{-2}) directly onto the Nafion HP membrane. A detailed procedure and a video of the deposition process can be found in our prior work.[21] Each catalyst-coated membrane had an electrode geometrical surface area of 10 cm^2 (31.6 mm × 31.6 mm). The membrane was mounted on a vacuum table heated at 85°C. The anode was deposited first and allowed to dry before the cathode CL was deposited on the other side of the membrane. In order to determine the Pt loading of the CLs, both the anode and cathode inks were sprayed onto a reinforced polytetrafluoroethylene (PTFE) decal. The final loading amount of Pt was calculated by weighing the PTFE decal before and after coating with the CL. This measurement was repeated 5 times, and the average was taken as the Pt loading. The performances of the prepared in-house CCMs were also compared to a commercially available CCM. The reference CCM was a Primea MESGA series CCM (active area: 25 cm^2, W.L. Gore & Associates A510.4/M710.18/C510.4) with a Pt loading of 0.10 mg_{Pt} cm^{-2} on the anode and 0.40 mg_{Pt} cm^{-2} on the cathode, separated by a 18 μm-thick PFSA-supported membrane. The properties of the in-house prepared CCMs used in PEMFC testing and the commercial Gore Primea-series CCM tested in this work are summarized in Table I.

Scanning electron microscopy of as-prepared CCMs.—Top view and cross-sectional images of the CCMs were recorded with a scanning electron microscope (SEM). To image the cross-section of the

CL, the CCM was secured between two pieces of Ni foil with conductive carbon tape and a section of the CCM was left to overhang from the edge of the Ni foil. The CCM|Ni foil was immersed in liquid N_2 for 2 min, removed, and the overhanging CCM was immediately cut with a fresh razor blade. The CCM|Ni foil was adhered to a 45/90° SEM stub with conductive carbon tape (Ted Pella, double coated). The exterior surface of the CL was imaged by cutting a small piece and adhering it to a standard SEM stub with conductive carbon tape. A Leo Supra 55 SEM with an accelerating voltage of 5 keV was used.

N_2-sorption porosimetry of as-prepared CCMs.—The size and volume of pores in the SSC Aquivion and LSC Nafion cathode CLs were determined by N_2-sorption porosimetry (Micromeritics ASAP2010 accelerated surface area and porosimetry analyzer). For the CCMs with LSC Nafion ionomer CLs, the samples used for these experiments are described in Table I (i.e. Prepared LSC Nafion for PEMFC testing). Separate CCMs from those tested in the PEMFC were prepared to probe the pore volume size distribution of the SSC Aquivion ionomer CLs. For the N_2-sorption porosimetry experiments, the SSC Aquivion ionomer was used in both the anode and cathode CLs; the properties of these CCMs are summarized in Table I. The as-deposited CCMs were cut into small strips and placed inside the porosimeter tube for degas at 100°C for 10 hours prior to characterization. Pore size distributions were calculated from adsorption isotherm data using Micromeritics DataMaster software. Micropore volume was derived from the t-plot fitted to Carbon STSA model. The total pore volume was determined at 0.98p/p0 and the pore size distribution was derived from the BJH method fitted to Harkins Jura equation.

MEA assembly for PEMFCs and fuel cell operation.—The cells were assembled by compressing the as-prepared CCMs with GDM in 10 cm^2 single cell test fixtures (single serpentine flow field, Fuel Cell Technologies). The thicknesses of the CCMs and GDMs were first measured with a digimatic micrometer (Mitutoyo, Model MDC-1" PX) at 9 evenly spaced locations over the component area and these measurements were averaged to calculate the component thickness and used to determine the required gasket thicknesses. We compress the MEAs in this study by 14%, which has been shown by our group[22,23] and others[24,25] to result in high performance at these operating conditions without significant MPL damage that can impart mass transport resistances. The CCMs were inserted between two 3M GDM and different thicknesses (4 and 5 mils) of virgin PTFE Skived Tape (Enflo) were used as gaskets. Average thicknesses of the wet-proofed anode and cathode GDM obtained from 3M were 266 ± 2 μm and 236 ± 4 μm, respectively. Cartridge heated end plates, current collectors, Poco graphite flow field with single serpentine flow channels, gaskets, GDMs, and the CCM were sealed together with 8 bolts torqued to 10 N m of torque per bolt in a star pattern. The Gore Primea MESGA CCM was made into a MEA by sandwiching between two wet-proofed 3M GDMs with different thicknesses of virgin PTFE Skived tape as gaskets and mounted into a 25 cm^2 fuel cell test fixture. Cartridge heated end plates, current collectors, Poco graphite flow fields with triple serpentine flow channels (Fuel Cell Technologies), gaskets, GDM, and the CCM were sealed together with 8 bolts torqued to 10 N m of torque per bolt in a star pattern.

Once assembled, the performance of single cells was tested using Scribner 850e fuel cell test systems from Scribner Associates, Inc. Experiments were conducted at a cell temperature of 80°C, pressures of ambient (101 kPa_{abs}) or 150 kPa_{abs} and relative humidities of 100% RH or 50% RH. Ultrapure gases (Ar, H_2, O_2, or Air, Alphagaz 2, Air-Liquide) were supplied to the anode and cathode under stoichiometric flow conditions of 2/10 for H_2/O_2 and 2/2 for H_2/Air, respectively. The H_2/Air flow was stoichiometric controlled at 2/2 for $J \geq 570$ mA cm^{-2} and at constant flow rate of 0.2 slpm for $J < 570$ mA cm^{-2}. All experiments started by breaking-in the MEA with the following sequence: the cell voltage was first held at 0.60 V in H_2/air for 2 hours, followed by 20 cycles alternating between 0.70 V and 0.40 V with each voltage held for 10 minutes. The polarization curves were obtained by measuring the current at various applied voltages (0.90, 0.88, 0.85, 0.80, 0.74, 0.70, 0.64, 0.60, 0.55, 0.50, 0.45, and 0.40 V); each voltage was held for 15 minutes, collecting 6 pts min^{-1}. The last 30 points were averaged for analysis purposes. Cell internal resistance was measured at current densities above 100 $mAcm^{-2}$ using the current interrupt technique with the load box and the Fuel Cell V.3.2 software (Scribner Associates Inc., Southern Pines, NC).

Fuel cell diagnostic measurements.—The electrochemically active Pt surface area (Pt ECSA) of the cathode electrode was evaluated via cyclic voltammetry (CV). CVs were carried out after cooling the cell temperature to 30°C and the gas temperatures to 50°C while flowing H_2|Ar at a flow rate of 0.2 slpm on the anode side and 0.05 slpm on the cathode, respectively, using a potentiostat to control the cell voltage (SI 1287, Solartron Analytical). The hydrogen-fed anode was used as both the reference electrode and counter electrode. The working electrode (cathode) potential was swept between 0.075 V and 1.15 V at a potential scan rate of 50 mV s^{-1} and reversed back to 0.075 V. The total charge for hydrogen adsorption was determined by integrating between a straight baseline drawn from the double layer capacitance region (0.40–0.50 V) and the final minimum in the cathodic (negative going) CV curve. A correction for double layer charging was done by subtracting the current observed at 0.40 V from the total current. The Pt ECSA was determined from the hydrogen adsorption charge and the characteristic value of charge density associated with a monolayer of hydrogen adsorbed on polycrystalline platinum, 210 μC cm^{-2}_{Pt}. The MEA catalyst utilization, U_{Pt}, was calculated by dividing the Pt ECSA measured by CV in an MEA to the intrinsic Pt ECSA of the catalyst measured by CV using a thin-film rotating disk electrode (RDE) in liquid electrolyte (i.e. 0.10 M $HClO_4$, Pt $ECSA_{RDE} = 86$ m^2 $g_{Pt}{}^{-1}$).[26] The H_2 cross-over current density was measured by linear sweep voltammetry (LSV) at a cell temperature of 80°C, under 0.2/0.05 slpm H_2/N_2, 100% RH at a rate of 1 mV s^{-1} from open circuit to 0.60 V.

The effective cathode proton transport resistance was determined after the MEAs were conditioned and polarization curves were measured. The cell temperature was held at 80°C and the inlet gas relative humidity was set to 50%. Hydrogen at the anode and nitrogen at the cathode were supplied at a constant flow rate of 0.2 slpm. The impedance spectra were collected with a Princeton Applied Research 263A potentiostat and a Solartron SI 1260 Impedance Analyzer. The amplitude of the sinusoidal current signal for the AC impedance was set at 5 mV over a frequency range of 2 kHz to 2 Hz. Data was measured logarithmically at 20 steps per decade. EIS spectra were obtained under a DC bias potential of 0.45 V versus the anode. Three spectra were measured to confirm reproducibility. The cathode proton transport resistance (i.e. $R_{H^+{}_{cath}}$ (Ω cm^2)) of the electrode was determined following a previously described procedure.[27] The proton resistivity of the CLs (i.e. $\rho_{H^+{}_{cath}}$ (Ω cm)) was calculated by dividing the cathode proton transport resistance by the thickness of the respective cathode CL determined using SEM. The proton conductance (i.e. $\rho_{H^+{}_{cath}}$ (S cm)) was calculated as the reciprocal of the proton resistivity.

EIS was also performed to determine the ohmic, charge transfer, and mass transport resistances among samples according to ionomer type used in the cathode CL. The EIS measurements were performed using the Scribner 850e fuel cell test systems (equipped with load and frequency analyzer). All electrochemical measurements were performed with a two-electrode cell with the anode used as a pseudo-reference electrode and measured after collecting the polarization curves used for data analysis. Three successive EIS measurements, each immediately preceded and followed by a 5 minute constant potential hold at the cell voltage of interest, were performed at 0.80 V, 0.60 V, and 0.40 V in potentiostatic mode to compare effective charge transfer resistances and mass transport limitations. The measurements were conducted under the same cell conditions as those used for the performance test: the same temperature, anode and cathode humidification temperature. However, EIS measurements were made at a constant flow rate. The flow rate was set 10% greater than the

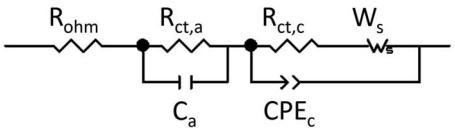

Figure 1. Equivalent circuit model (ECM) used in this work to fit Nyquist spectra presented in Figure 7.

current measured at the cell voltage of interest in the polarization curve collected before measuring EIS to avoid an artificial mass transport resistance that may be induced by flow controllers responding out of phase to perturbations in the DC current in the impedance measurement. The EIS measurements ranged from 10,000 to 0.1 Hz following a 5 minute hold at the selected cell voltage with an AC current equal to 2% of the DC current.

The equivalent circuit model (ECM) of Zhai et al.[28] was used to analyze the contributions to the impedance spectra of the anode and cathode kinetic and mass transport processes. This ECM is shown in Figure 1, and includes a serial resistance and an anode and cathode model. R_{ohm} represents the serial resistance of the proton and electron transport of the bulk system. The anode model includes a charge transfer resistance of the hydrogen oxidation reaction, $R_{ct,a}$, and a capacitance of the anode CL, C_a. The cathode model includes a charge transfer resistance for the ORR, $R_{ct,c}$, a constant phase element (CPE_c) and a finite length, Warburg diffusion element, W_s. The ECM in Figure 1 was used to simulate the impedance data in the later section of this paper using ZView 2 software (Scribner Associates).

The total mass transport resistance was derived from limiting current measurements at different total pressures and varied O_2 concentrations.[2] To maintain uniform down-the-channel conditions, high stoichiometries were used. On the anode side, 1.0 slpm of H_2 flowed at all cell conditions. O_2 stoichiometries exceed 10 at all test points by flowing O_2/N_2 mixtures at a flow rate of 1.5 slpm. With the cell operating temperature maintained at 80°C, dry O_2 mole fractions of 0.5%, 1.0%, 1.5%, 2.0%, and 2.5% in N_2 were used to measure the limiting current. For each gas mixture, the following anode and cathode total pressures were used to consider pressure dependence: 110 kPa_{abs} (80% inlet gas RH), 150 kPa_{abs} (71% inlet gas RH), 200 kPa_{abs} (67% inlet gas RH), and 300 kPa_{abs} (64% inlet gas RH). The cell voltage was scanned from 0.30 V to 0.06 V in 30 mV steps with 2 minute cell voltage holds in order to measure the limiting currents for each diluted O_2 mixture and at each total pressure. The limiting currents selected for analysis were the maximum current measured in this cell voltage range prior to current decrease at the lowest cell voltages.[29] The total O_2 mass transport resistance was calculated by using Equation 3 from Baker et al.[29]

Results and Discussion

Microstructure of the SSC Aquivion and LSC Nafion CLs.— SEM images of the outer surface of MEAs utilizing the SSC Aquivion and LSC Nafion ionomer in the cathode CL are presented in Figure 2 at two magnifications. The CL surface (Figs. 2a and 2b) did not present any cracks or mud-like morphologies that are typically observed for CLs prepared by screen printing or spraying. In the high magnification SEM images (Figs. 2c and 2d), the structures of the CLs are similar for both CCMs under study, and comprise an interconnected network of ~100-nm carbon particles with 2-to-5 nm Pt particles and 10-to-200 nm pores. Fig. 2e and Fig. 2f show the cross-section images of a Nafion HP membrane coated on one side by the respective CL. The CLs presented in this work are highly uniform in thickness and in contact with the Nafion HP membrane. For the MEA comprising the SSC Aquivion ionomer in its cathode CL, the CL thickness is 7.8 μm at 0.31 mg_{Pt} cm^{-2} according to the SEM investigations, seen in Figure 2e. The cathode CL thickness of the MEA comprised of the LSC Nafion ionomer, shown in Fig. 2f, is similar (i.e. 8 μm) to that of the SSC Aquivion ionomer-based cathode CL at the same Pt loading, suggesting similar macroscopic morphologies between the Aquivion and Nafion-based CL.

While the SEM images of the CCMs with SSC Aquivion and LSC Nafion-based CLs are similar, their pore volume size distribution curves are vastly different, as presented in Figure 3 and Table II. Both CLs are comprised of smaller primary micropores ranging from 2–10 nm in diameter and larger secondary mesopores ranging from 20–110 nm in diameter (Figure 3). The smaller pores are attributed to the space in and between the primary particles in the carbon agglomerate (mixture of intraparticle and interparticle pores), while the larger ones are attributed to interparticle pores between carbon agglomerates only.[30] Similar pore size distributions were reported by Suzuki et al.[31] for CLs prepared with the doctor blade method and Yu et al.[32] for CLs prepared with reactive spray deposition technology. The total pore volume for both CLs under study is identical at 1.2 $m^3/g_{C\ cathode}$.

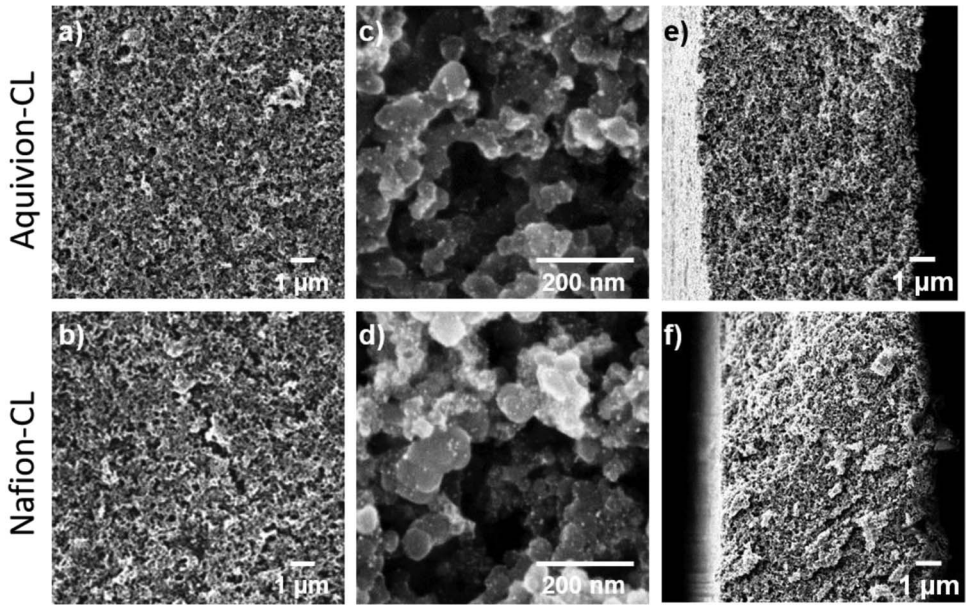

Figure 2. Plane-view SEM images of the MPL-facing surface of the a) SSC Aquivion CLs and b) LSC Nafion CLs. High magnification SEM images of c) SSC Aquivion CLs and d) LSC Nafion CLs. Cross-sectional SEM images of e) SSC Aquivion CLs and f) LSC Nafion CLs.

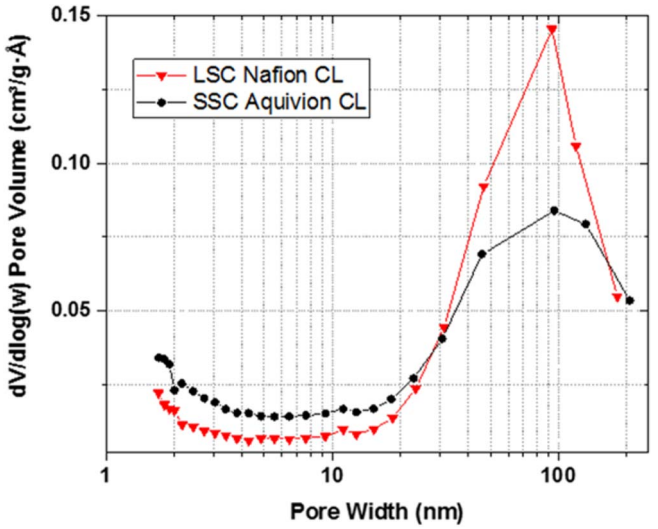

Figure 3. Pore volume size distribution of SSC Aquivion CLs and LSC Nafion CLs. See Table I for more information on the CL compositions.

A significant difference between the two CLs is that the SSC Aquivion CL has a higher micropore volume, while the LSC Nafion CL has a higher mesopore volume, indicating significant structural differences between the CLs. The micropore volume is $0.087 m^3/g_{CB\ cathode}$ for the CL that utilizes the SSC Aquivion ionomer compared to $0.026\ m^3/g_{CB\ cathode}$ for that with the LSC Nafion ionomer. The BET surface area for CLs with the SSC Aquivion ionomer ($652\ m^2/g_{CB\ cathode}$) is two times greater than CLs with the LSC Nafion ionomer ($354\ m^2/g_{CB\ cathode}$). Being that the anodes for these 2 types of CCMs are identical to their respective cathodes, the results imply that the CCM with the SSC Aquivion CL has about 2 times higher surface area than that with the LSC Nafion-containing cathode CL. The higher micropore volume for the CCMs with the SSC Aquivion CL indicates less filling of the pores in the range of 2 to 10 nm by the SSC Aquivion ionomer. As a result, the primary pores of the carbon support in the CL containing the SSC Aquivion ionomer are more hydrophobic than those in the LSC Nafion CL, which is expected to improve reactant transport and water removal in the former.[5,6]

Pt electrochemical surface area and proton resistance in the CLs.—Representative CVs recorded for the PEMFCs utilizing the SSC Aquivion and LSC Nafion ionomer in the cathode CLs are shown in Figure 4a. The CVs recorded for each of cathode CLs under study exhibit the same distinguishing features of hydrogen adsorption/desorption between 0.075 V and 0.40 V and oxide layer formation between 0.60 V and 1.15 V. These signature peaks are typical for CLs containing Pt/CB catalysts. The different hydrogen adsorption/desorption charges are quantitatively shown by the corresponding Pt ECSA and U_{Pt} values in the bar chart in Figure 4b. The Pt ECSA values presented in Fig. 4b correspond to the average values calculated for eight individual PEMFCs utilizing the SSC Aquivion ionomer and LSC Nafion ionomer, respectively, in the cathode CLs.

Table II. Summary of N_2 sorption porosimetry results of the SSC Aquivion and LSC Nafion CLs. See Table I for more information on the CCM compositions.

	SSC Aquivion CL	LSC Nafion CL
BET surface area ($m^2/g_{CB\ cathode}$)	652	354
Micropore surface area ($m^2/g_{CB\ cathode}$)	206	70
Total pore volume ($cm^3/g_{CB\ cathode}$)	1.2	1.2
Micropore volume ($cm^3/g_{CB\ cathode}$)	0.087	0.026

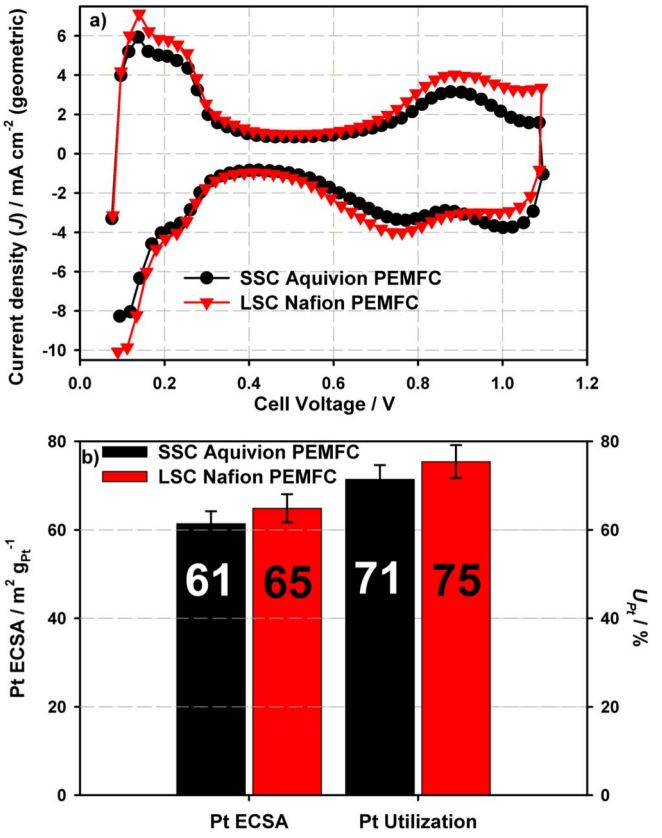

Figure 4. a) Typical cyclic voltammograms (CVs) recorded for the SSC Aquivion PEMFCs (black circles) and LSC Nafion PEMFCs (red down triangles). CVs recorded at cell temperature of 30°C, under an environment of H_2 /N_2 (both at 50°C) at flow rates of 0.2/0.05 slpm and potential scan rate of 50 mV s^{-1}. b) Pt ECSA values and Pt utilization (U_{Pt}) of SSC Aquivion PEMFCs and LSC Nafion PEMFCs.

The error bars correspond to the standard deviation for the eight independent CV measurements. The Pt ECSA values calculated from the hydrogen adsorption charges at 100% RH are identical for the cathode CLs containing the SSC Aquivion ionomer and the cathode CLs containing the LSC Nafion ionomer ($61 \pm 3\ m^2\ g_{Pt}^{-1}$ and $65 \pm 3\ m^2\ g_{Pt}^{-1}$, respectively). Similar observations were reported by Lei et al.[14] and Choo et al.[17] The U_{Pt} values calculated from the Pt ECSA values were 71 ± 3% and 75 ± 4% for the cathode CLs containing the SSC Aquivion ionomer and the cathode CLs containing the SSC Nafion ionomer, respectively. This is in contrast to Park et al.[16] who reported higher Pt ECSA values for their Pt/GCB (graphitized carbon black) CCMs utilizing SSC ionomers in the cathode CLs compared to the control LSC Nafion CCMs; the U_{Pt} values for the SSC MEAs were between 3 to 10% higher compared to LSC Nafion CCMs. Park et al.[16] stated that the increase in U_{Pt} values indicates an increased accessibility of the SSC ionomers to the graphitized carbon surface and Pt nanoparticles.

The results of the protonic conductivity measurement for the different PEMFCs by in situ EIS is shown in Figure 5 under an operating cell temperature of 80°C in flowing H_2/N_2 at the anode/cathode at 50% inlet gas RH. The cathode proton transport resistance, $R_{H+,cath}$, is lower for the SSC Aquivion PEMFC ($0.011\ \Omega\ cm^2$) compared to when LSC Nafion PEMFC ($0.027\ \Omega\ cm^2$) is used as the ionomeric binder. This is consistent with previous results for SSC ionomers at similar loadings to LSC counterparts and is related to the higher ion exchange capacity of the former and its improved capacity for proton conduction.[14] The $R_{H+,cath}$ for the different cathode CLs, along with proton resistivity (i.e. ρ_{H^+cath}) proton conductance (i.e. σ_{H^+cath}), and CL thicknesses are listed in Table III.

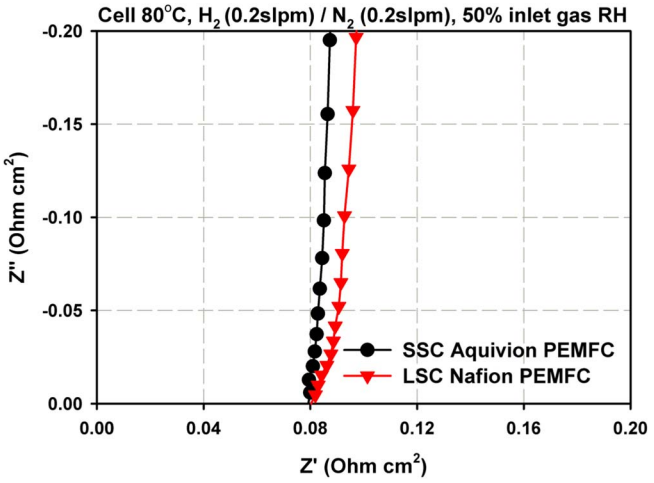

Figure 5. Protonic impedance of cathode CLs containing SSC Aquivion (black circles) and LSC Nafion PEMFCs (red down triangles) operated under H_2 (0.2 slpm)/N_2 (0.2 slpm) at cell temperature of 80°C and 50% inlet gas RH.

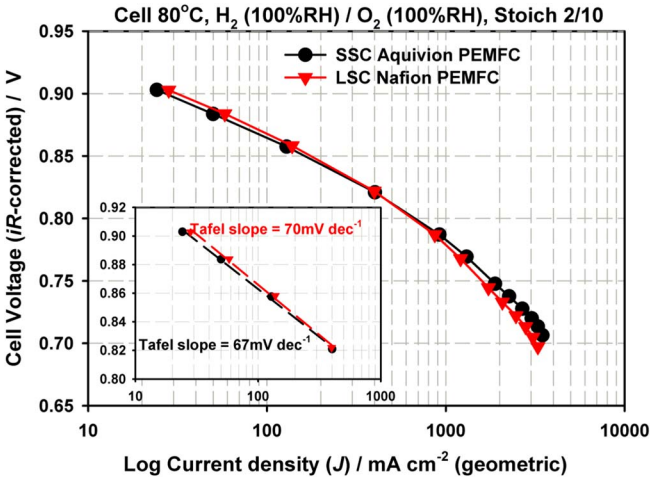

Figure 6. H_2/O_2 I-V polarization curves recorded at cell temperature of 80°C, ambient pressure, 100% RH (anode/cathode) and at a stoichiometric flow rate of 2/10, corrected for *iR drop* as well as by the H_2 crossover current. Inset: Tafel region.

Single-cell testing of SSC Aquivion and LSC Nafion PEMFCs.— In the absence of any ohmic and mass transport losses in the fuel cell, the inherent electrode kinetics of the two types of cathode CLs with regards to the ORR are similar under fully humidified conditions. Figure 6 presents the *iR*-corrected Tafel plots for the average current-voltage (I-V) polarization curves recorded in H_2/O_2 at 2/10 stoichiometric flow rates at an operating cell temperature of 80°C and an inlet RH value of 100%. The corrected cell voltage ($V_{corrected} = V_{cell} + iR\ drop$) obtained from the polarization plots for the PEMFCs tested is plotted against the current density corrected for H_2 crossover current (i.e 4 ± 0.5 mA $cm^{-2}{}_{geometric}$) on a logarithmic scale. In the kinetically controlled regime (from 0.90 V to 0.80 V) at 100% RH, the Tafel slope measured for the PEMFCs with SSC Aquivion in the cathode CL (66 mV dec^{-1}) and for the LSC Nafion-based PEMFCs (70 mV dec^{-1}) are very similar to each other. This similarity suggests that the ionomer type (SSC Aquivion vs. LSC Nafion) does not exert an influence on the ORR kinetics. These Tafel slopes are close to the theoretical value of 70 mV dec^{-1} at 80°C for a chemical step following the first electron transfer as the rate determining step under Temkin adsorption conditions.[33] This result is in contrast to Park et al.[16] and Lei et al.[14] who reported higher Tafel slopes for their SSC PEMFCs compared to their LSC Nafion PEMFCs at identical cell temperature and relative humidity. Park et al.[16] ascribed the higher Tafel slopes measured for their SSC PEMFCs to an increase of O_2 diffusion resistance from the gas phase to the catalyst sites as a result of excess water in the cathode CL. The polarization curves shown in Figure 6 for PEMFCs with either cathode CL ionomer are nearly straight lines over two decades of current densities (10–1000 mA cm^{-2}), indicating good O_2-transport properties for the electrodes. The ORR mass activity values (i_m) at an operating cell voltage of 0.90 V for the PEMFCs utilizing the SSC Aquivion and LSC Nafion ionomer in the cathode CLs were extracted from Figure 6 and are summarized in Table III. As can be seen, the mass activities of the PEMFCs utilizing the SSC Aquivion and LSC Nafion ionomer in the cathode CLs are essentially identical and are in good accordance with literature values reported for Pt catalyst supported on carbon black.[2,26,34]

Figures 7a and 7b compare the average polarization and power density curves measured for eight different PEMFCs containing the SSC Aquivion ionomer in the cathode CL (black circle, black error bar) to the average polarization curve measured for eight different PEMFCs containing the LSC Nafion ionomer in the cathode CL (down-red triangle, red error bar) at 80°C and fed with ambient pressure air, humidified at 100% RH and 50% RH, respectively. The error bars correspond to the standard deviation for the eight individual polarization curve measurements. The typical polarization and power density curves (green square, no error bar) recorded for the reference Gore PEMFC is also included in Figure 7 for comparison. The PEMFCs utilizing the SSC Aquivion ionomer in the cathode CL are identical to that of the standard Gore PEMFC over the entire voltage range. However, there are significant differences in the performance of the SSC Aquivion vs. the LSC Nafion PEMFCs when operating at 80°C in air at ambient pressure at 100% RH and 50% RH. When the RH of the supplied gases is set at 100% RH, in the kinetic region of the polarization curve (i.e. cell voltage ≥ 0.80 V), in which there is a smaller effect of mass transport, PEMFC performances are very similar for the two types of cathode CLs under study.

The average current density observed at an operating cell voltage of 0.80 V is 173 ± 11 mA cm^{-2} for PEMFCs with cathode CLs containing the SSC Aquivion ionomer, 185 ± 9 mA cm^{-2} for PEMFCs with cathode CLs containing the LSC Nafion ionomer and 151 mA cm^{-2} for the Gore PEMFC. The fact that PEMFC performance at high cell voltages is insensitive to the ionomer in the cathode CL matches observations previously reported in the literature[14–16] as described in this paper's introduction.

When the RH of the supplied gases is reduced to 50% RH, the PEMFC performance at high cell voltage is very similar for the two cathode CL ionomers tested in this study. The average current density observed at an operating cell voltage of 0.80 V is 195 ± 12 mA cm^{-2} for cathode CLs containing the SSC Aquivion ionomer, 187 ± 14 mA cm^{-2} for cathode CLs containing the LSC Nafion ionomer and 152 mA cm^{-2} for the Gore PEMFC. A similar behavior is observed by Lei et al.[14] when testing their PEMFCs at 80°C and 70% RH–the PEMFCs

Table III. Summary of Cathode CL thicknesses, cathode proton transport resistance ($R_H{}^+{}_{cath}$), cathode proton resistivity ($\rho_H{}^+{}_{cath}$), cathode proton conductance ($\sigma_H{}^+{}_{cath}$) and mass activities (i_m) for the two types of CL under study.

	CL Thicknesses μm	$R_H{}^+{}_{cath}$ Ω cm^2	$\rho_H{}^+{}_{cath}$ Ω cm	$\sigma_H{}^+{}_{cath}$ S cm^{-1}	i_m A $mg_{Pt}{}^{-1}$
SSC Aquivion PEMFC	7.8	0.0107	13.4	7.49	0.110
LSC Nafion PEMFC	8.0	0.0274	34.3	2.92	0.093

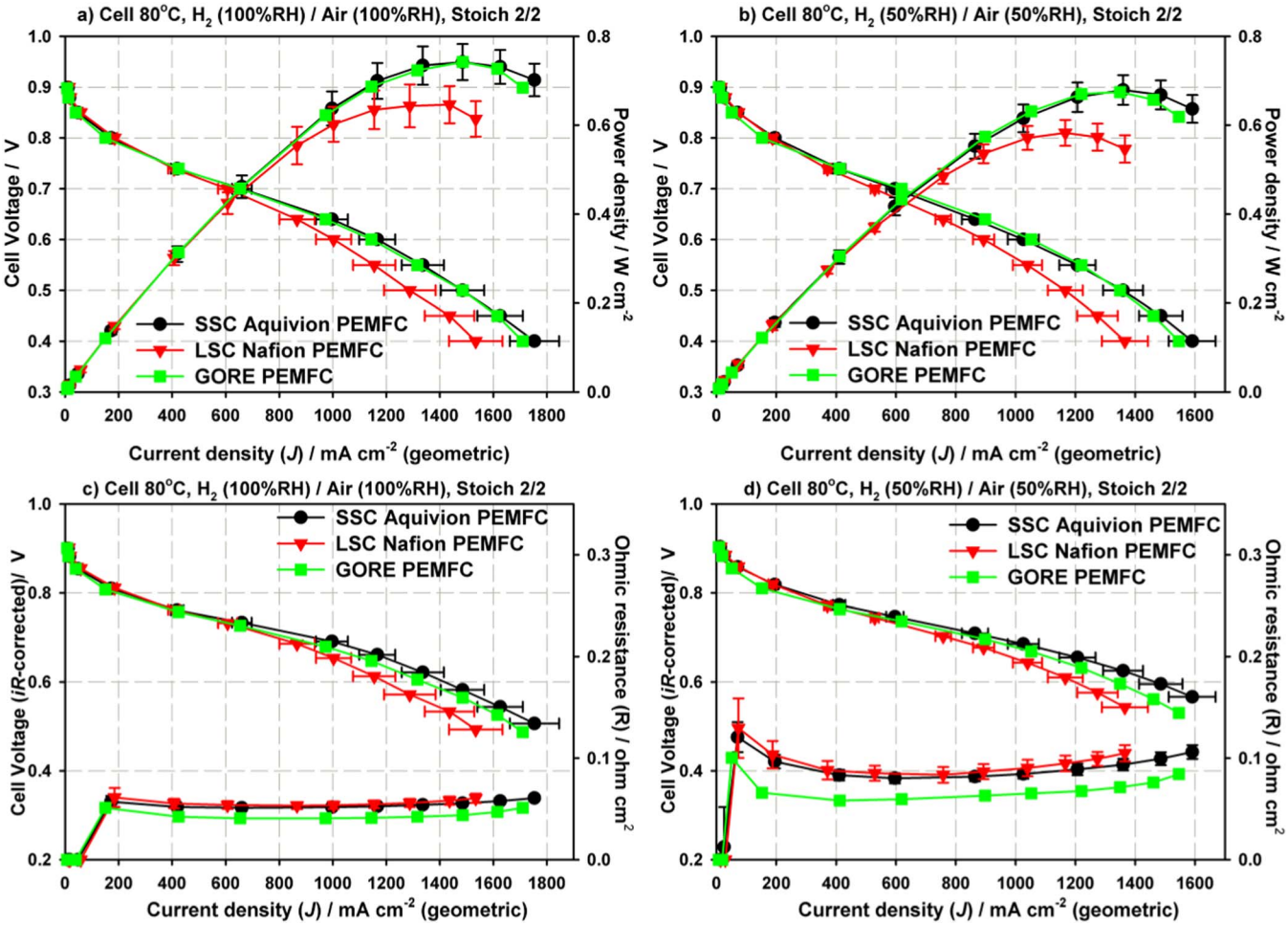

Figure 7. Comparison of the average I-V polarization and power density curves obtained for eight SSC Aquivion PEMFCs to the average I-V polarization and power densities obtained for eight LSC Nafion PEMFCs at a cell temperature of 80°C, ambient pressure at a) 100% RH and b) 50% RH. The error bars correspond to the standard deviation for the 8 independent measurements. The polarization and power density curves recorded for the reference Gore PEMFC are also added to the figure for comparison. *iR*-corrected I-V polarization curves and ohmic resistances measured at a cell temperature of 80°C, at ambient pressure, and at c) 50% RH and d) 100% RH.

containing the SSC Aquivion ionomer in their cathode CL achieved the same cell voltages as the PEMFCs containing the LSC Nafion ionomer.

The differences in cell performance between the PEMFCs with two types of cathode CL ionomer are more pronounced at lower cell voltage (i.e. the high current density region at cell voltage ≤ 0.60 V) at both 100% RH and 50% RH. The PEMFCs containing the SSC Aquivion ionomer in the cathode CLs have higher current densities at lower cell voltages, requiring a higher consumption of O_2 and H^+, compared to the PEMFC containing the LSC Nafion ionomer in the cathode CLs. The advantage of a lower cathode proton transfer resistance, observed in Figure 5 for the SSC Aquivion cathode CLs, is one reason that the PEMFCs containing the SSC Aquivion ionomer exhibit a higher cell performance than the PEMFCs containing the LSC Nafion ionomer at $J \geq 550$ mA cm^{-2} (i.e. cell voltage $\leq$0.70 V) at both 100% RH and 50% RH. In contrast, reports in the literature at similar cell conditions studying the influence of cathode CL ionomer do not report an advantage to using SSC Aquivion ionomer in the CL until much higher current densities ($J \geq 800$ mA cm^{-2}).[14–16]

In our PEMFCs, we observe that the addition of the SSC Aquivion ionomer in the cathode CL improves performance at both low (50% RH) relative humidity and in fully humidified (100% RH) conditions. When operating the cell at 80°C, ambient pressure and 100% RH, the average current densities for the PEMFCs measured at an operating cell voltage of 0.60 V are 1166 ± 67 mA cm^{-2} for PEMFCs containing the SSC Aquivion ionomer in the cathode CL, 1003 ± 65 mA cm^{-2} for PEMFCs containing the LSC Nafion ionomer and 1145 mA cm^{-2} for the reference Gore PEMFC. The average peak power densities measured for the PEMFC containing the SSC Aquivion ionomer, the PEMFC containing the LSC Nafion ionomer, and the reference Gore PEMFC are 0.742 ± 0.041 W cm^{-2}, 0.646 ± 0.042 W cm^{-2}, and 0.742 W cm^{-2}, respectively. A 1.15 × higher cell power density was observed for the PEMFC containing the SSC Aquivion ionomer when compared to PEMFC containing the LSC Nafion ionomer in the cathode CL. After reducing the inlet relative humidity to 50% at the same cell temperature, pressure, and gas flow conditions, the average current densities and power densities measured at 0.60 V are 1025 ± 52 mA cm^{-2} and 0.679 ± 0.041 W cm^{-2} for the PEMFCs containing the SSC Aquivion ionomer, 893 ± 35 mA cm^{-2} and 0.582 ± 0.042 W cm^{-2} for PEMFCs containing the LSC Nafion ionomer, and 1052 mA cm^{-2} and 0.674 W cm^{-2} for the reference Gore PEMFC. This 17% increase in power density of our PEMFCs with the SSC ionomer over those with LSC-containing CLs is somewhat surprising, as the same membrane, anode and cathode GDM, catalyst (i.e. 50 wt% Pt/CB), and catalyst loading (0.31 mg$_{Pt}$ cm^{-2}) are used for both sets of experimental cathode CLs in this study, similarities which would normally engender very similar fuel cell performance.

We find that when the SSC Aquivion ionomer is used in the cathode CL, the PEMFC performance improvements at intermediate current densities that are observed at moderate RH also persist when fully

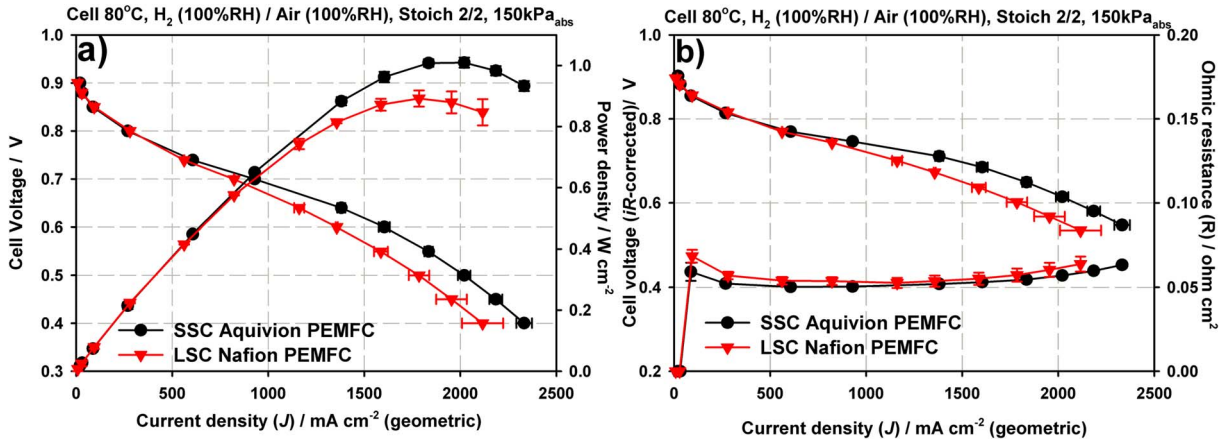

Figure 8. a) Comparison of the average I-V polarization and power density curves obtained for four SSC Aquivion PEMFCs to the average I-V polarization and power densities obtained for four LSC Nafion PEMFCs at cell temperature of 80°C, 100% RH (anode/cathode) and 150 kPa_{abs} back pressure and b) *iR*-corrected I-V polarization curves and ohmic resistances.

humidified gases are used (100% RH). Contrary to these observations, Park et al.[16] have reported that at 100% RH and at a cell operating voltage of 0.60 V, PEMFCs prepared with SSC Aquivion ionomer in the cathode CL showed lower current densities than the PEMFCs with LSC Nafion ionomer in the cathode CL; the authors attributed this reduction in performance at high RH to excessive swelling of the more hydrophilic SSC Aquivion ionomer. At low RH, Park et al.[16] observed that the current densities for PEMFCs with Aquivion ionomer CLs were higher than those of PEMFCs prepared with the LSC Nafion ionomer in the cathode CLs due to higher proton conductivity and water uptake in the former.

Like the I-V polarization curves obtained at ambient pressure, the SSC Aquivion PEMFCs outperform the LSC Nafion PEMFCs under backpressure, or conditions for which mass transport resistances are significantly reduced. Figure 8a compares the average polarization and power density curves measured for three different PEMFCs containing the SSC Aquivion ionomer in their cathode CLs (black circles, black error bars) to the average polarization curve measured for three different PEMFCs containing the LSC Nafion ionomer in the cathode CLs (red down triangles, red error bars) at 80°C, fed with 150 kPa_{abs} back pressure H_2 and air and humidified at 100% RH. The error bars correspond to the standard deviation for the three individual polarization curve measurements. At an operating cell voltage of 0.60 V, the average current density and peak power density measured for the SSC Aquivion PEMFCs are 1604 ± 29 mA cm^{-2} and 1.01 ± 0.02 W cm^{-2} compared to 1357 ± 10 mA cm^{-2} and 0.892 ± 0.03 W cm^{-2} for the LSC Nafion PEMFCs. *iR*-corrected polarization curves (i.e. Figure 8b), in which contribution from the bulk membrane resistance is removed, also exhibit significantly different performances for the two cathode CL ionomers. This indicates that there are additional sources of resistance in the LSC Nafion PEMFCs contributing to the reduced performance, not solely its higher ohmic resistance, compared to when SSC Aquivion ionomer is used at the cathode CL.

An O_2-gain voltage experiment can be used to estimate the mass transport resistance loss associated with operating the fuel cell with air supplied to the cathode, because the cathode suffers negligible mass transport loss when pure O_2 is used as the oxidant. The O_2-gain voltage is calculated from the difference in *iR*-corrected potentials at given current densities when the cathode is fed pure O_2 and air, and it provides insight into the degree of O_2 mass-transport resistance within a fuel cell.[18,35] As seen in Figure 9a, at a current density ≥ 500 mA cm^{-2}, the O_2-gain voltage of the PEMFC using the LSC Nafion ionomer in its cathode CL increases rapidly with increasing current density compared with the PEMFC using the SSC Aquivion ionomer in its cathode CL, indicating a rapid increase of the O_2 diffusion resistance in the former. The lower O_2-gain voltage for the PEMFC with SSC Aquivion ionomer in the cathode CLs suggests that use of this ionomer establishes a well-balanced supply path of protons and O_2 in the high current density region, where the reactant transport is the rate-limiting step. Its lower O_2-gain voltage might be evidence of a more uniform ionomer distribution and coverage when SSC Aquivion ionomer is used.[16]

Figure 9b presents calculated total O_2 transport resistance (R_{total}) as a linear function of the total gas pressure and supports the result from the O_2-gain voltage experiments in Figure 9a that PEMFCs containing SSC Aquivion in the cathode CL have considerably lower O_2

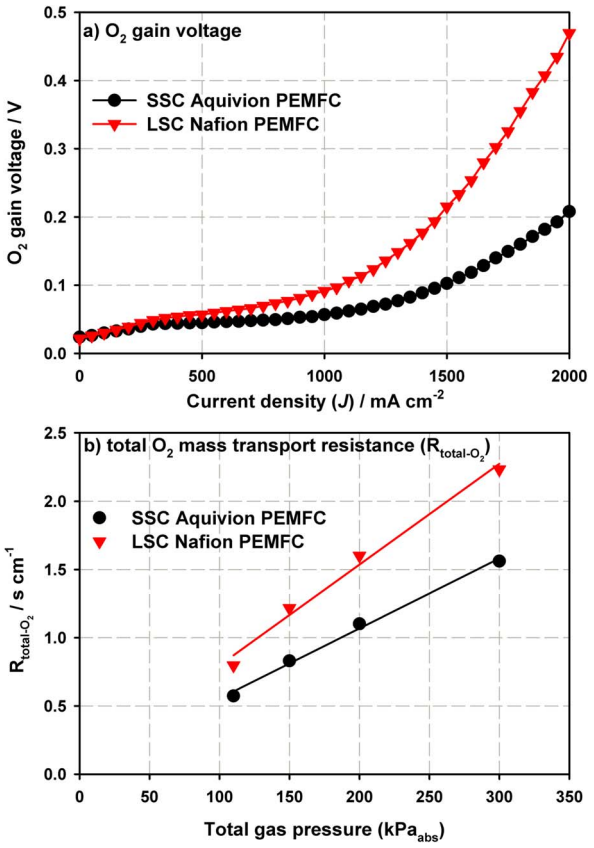

Figure 9. a) Comparison of O_2 gain voltage for SCC Aquivion PEMFCs to LSC Nafion PEMFCs measured at cell temperature of 80°C, 100% RH (anode/cathode) and ambient pressure. b) Comparison of total O_2 transport (R_{total}) resistance as a function of total gas pressure.

transport resistance. The total O_2 transport resistance for PEMFCs containing the SSC Aquivion in the cathode CL is ∼30% lower than for LSC Nafion. This result, along with the improvement in cathode H^+ transport (Figure 5, Table III), explains the marked performance improvement seen in the former at all operating conditions tested in this study beyond intermediate current densities. Additionally, PEMFCs containing the SSC Aquivion in the cathode CL have a $R_{total\text{-}O2}$ that is less pressure-dependent–apparent from the lower slope of $R_{total\text{-}O2}$ vs. total pressure data–than the LSC Nafion PEMFCs, which indicates an improvement in intermolecular gas diffusion through the cathode GDM and gas channels.[2,29,36] Since the same GDM are used for all measurements, one would expect any differences observed to originate from the changes in the CLs and that the direct contributions from the diffusion media and the microporous layer remain unchanged. Therefore, we attribute this effect to the increase in microporosity shown in Figure 3 for the SSC Aquivion cathode CLs that is expected to facilitate liquid water evaporation in the CL.[5,6]

The in-situ EIS measurements provide more insight into the role of the SSC ionomer in the cathode CL. Impedance spectra measured at 100% RH are shown on the left side of Figure 10 and the impedance spectra measured at 50% RH are shown on the right side. These results are expressed using a Nyquist plot in rectangular coordinate form, which consists of a real part and an imaginary part with phase angle. The intersection of the spectra on the x-axis at the high frequency domain is attributed to ohmic resistance (R_{ohm}), which is primarily from the ionic resistance in the electrolyte and the CL. Qualitatively, the difference between the low frequency intercept and the high frequency intercept on the real impedance axis (i.e. the diameter of the spectra R_{total}) is the sum of the effective charge transfer resistances at the anode and cathode ($R_{ct,a}$ and $R_{ct\text{-}c}$) and the mass transport resistance (R_{mt}). R_{total} mostly consists of cathode charge transfer ($R_{ct,c}$) limited resistances at lower current densities (i.e. operating cell voltage of 0.80 V) since the O_2 consumption rate is small but contains contributions from O_2 transport resistance (R_{mt}) at higher current densities (i.e. operating cell voltage of 0.60 V and 0.40 V). Similar spectra have been widely reported in the literature for PEMFCs.[9,14,37] At a cell operating voltage of 0.80 V, the impedance spectra are dominated by a high-frequency feature, indicating that the reaction process is limited by the kinetics. While the effective charge transfer resistance is largely dominated by the rate of the interfacial ORR process, the H^+ conduction and O_2 permeability limitations within the CL also contribute.[9] As the overpotential increases (i.e. operating cell voltage ≤ 0.60 V), the feature at low frequency becomes more significant, suggesting that the reaction process may be limited by O_2 mass-transfer to the CL. This transition can be observed in Figure 10, as the feature at high frequency shrinks and the low frequency feature expands as the cell voltage is decreased. Similar behavior has been widely observed in the literature.[9,14,37]

The fit results from the ECM (model shown in Figure 1) are shown as solid lines in Figure 10. For nearly the entire frequency range, the simulation data of the ECM fit well to each cell response under each test condition. The R_{ohm} response is clearly visible at the high frequencies in the impedance spectra. The $R_{ct,a}$ and C_a in the anode model contributed to the smallest impedance arc at the highest frequencies. The $R_{ct,c}$ and CPE in the cathode model contributed to the large arc at intermediate frequencies. The feature at the lowest frequencies is attributed to the finite length Warburg diffusion element, W_s, which corresponds to the mass transport resistance to O_2 diffusion to the cathode CL when the cell is operated at high current densities. All resistances derived from the ECM fitting are shown in Figures 11a and 11b for 100% and 50% RH, respectively. The fitting error is less than 6% for all parameters.

Figures 11a and 11b show that no significant differences in the ohmic resistances (R_{ohm}) are observed between the two sets of PEMFCs under study. At both RH, R_{ohm} values remain relatively constant when changing the cell operating voltage from 0.80 V to 0.60 V and 0.40 V, matching our measurements by current-interrupt shown in Figure 7c. At 50% RH, R_{ohm} are higher than at 100% RH since the membranes are less hydrated. At the cell operating voltage of 0.80 V and cell temperature of 80°C at either inlet relative humidity, charge transfer resistance ($R_{ct,c}$) contributes the most to the total impedance for both PEMFCs under study. As the cell operating voltage changes from 0.80 V to 0.60 V, $R_{ct,c}$ increases for the LSC Nafion PEMFCs from 0.296 Ω cm^2 to 0.593 Ω cm^2. Such an increase in charge transfer resistance at higher cell current densities has been attributed to both poor proton conductivity through the CL ionomer and a decrease in O_2 concentration within the CL as a result of O_2 transport limitations,[9] consistent with our observations of higher cathode H^+ transport resistance and greater total O_2 mass transport resistance for the Nafion-based PEMFCs in Figures 5 and 9, respectively. In contrast to the PEMFCs with LSC Nafion ionomer in the cathode CL, the $R_{ct,c}$ values remain unchanged for the SSC Aquivion PEMFCs as the cell operating voltage changes from 0.80 V to 0.60 V. At the cell operating voltage of 0.60 V, the CLs containing the SSC Aquivion ionomers have about half the charge transfer resistance as ones with LSC Nafion ionomer. We consider that this could be the result of decreased local flooding from accumulated liquid water, leading to increased O_2 diffusion through the CL, or increased proton conduction in the CLs containing SSC Aquivion ionomer. The lower O_2-gain voltage and $R_{total\text{-}O2}$ in Figure 9a and Figure 9b supports the conclusion that the SSC Aquivion ionomer improves O_2 diffusivity to the active sites. The higher micropore volume of the PEMFCs with SSC CLs (Figure 3) suggests that better water management, and lack of liquid water, is the reason for the decrease in the charge transfer resistance and improvements in performance with use of the SSC Aquivion ionomer in the cathode CL. The $R_{ct,c}$ values measured for the SSC Aquivion PEMFCs at 50% RH are also lower than at 100% RH, whereas the Rct-c values measured for the LSC Nafion PEMFCs are fairly constant under these tested conditions, suggesting that the SSC ionomer facilitates water management over a range of RHs.

The mass transport resistance becomes a larger contributor to the cell resistance at the cell operating voltage of 0.40 V for both sets of PEMFCs under study. Note that fuel cells are rarely operated at this low potential at which their efficiency is poor, but transients to this voltage are likely. The EIS shows that the improved electrical performance of the PEMFCs with the SSC-containing cathode CLs is related to a lower mass transport resistance relative to PEMFCs with the LSC Nafion ionomer. In this high current density region, the production of water is high, and the PEMFCs with SSC Aquivion in the cathode CL appear better equipped to reject liquid water due to higher micropore content, and thus have less resistance to mass transport. Fitting the results to advanced models of micropores and water evaporation will be useful to confirm these theories.

Conclusions

We can clearly conclude that using SSC Aquivion ionomers in the cathode CL of PEMFCs leads to superior I-V polarization curves, lower cathode H^+ transport resistance, lower O_2-gain voltage, lower charge-transfer resistance for the ORR, and lower mass-transport resistance as compared to PEMFCs containing LSC Nafion ionomers in the CLs. The improvement imparted by the SSC ionomers is not observed at lower current densities, or the kinetic region around 0.80 V, but rather under more mass transport limited conditions at 0.60 V and 0.40 V, and persists at all cell operational conditions (50% and 100% RH). Our uniformly higher performance for PEMFCs with SSC-containing CLs is unlike many reports in the literature that see benefits for using SSC ionomers in the cathode CL only in hot and dry conditions. Albeit direct comparison to previous work in the literature is difficult due to the number of variables related to cell construction, and our I-V polarization curves are higher in general than those reported in the literature. Though this may be related to lower Pt loadings used in some other reports, we also consider that ink preparation and formulation and/or non-optimal GDM selection and compression may affect water management in the CL that could result in differences in I-V polarization curves.

We can attribute the uniform I-V performance improvement in the PEMFCs containing SSC Aquivion ionomer to materials property

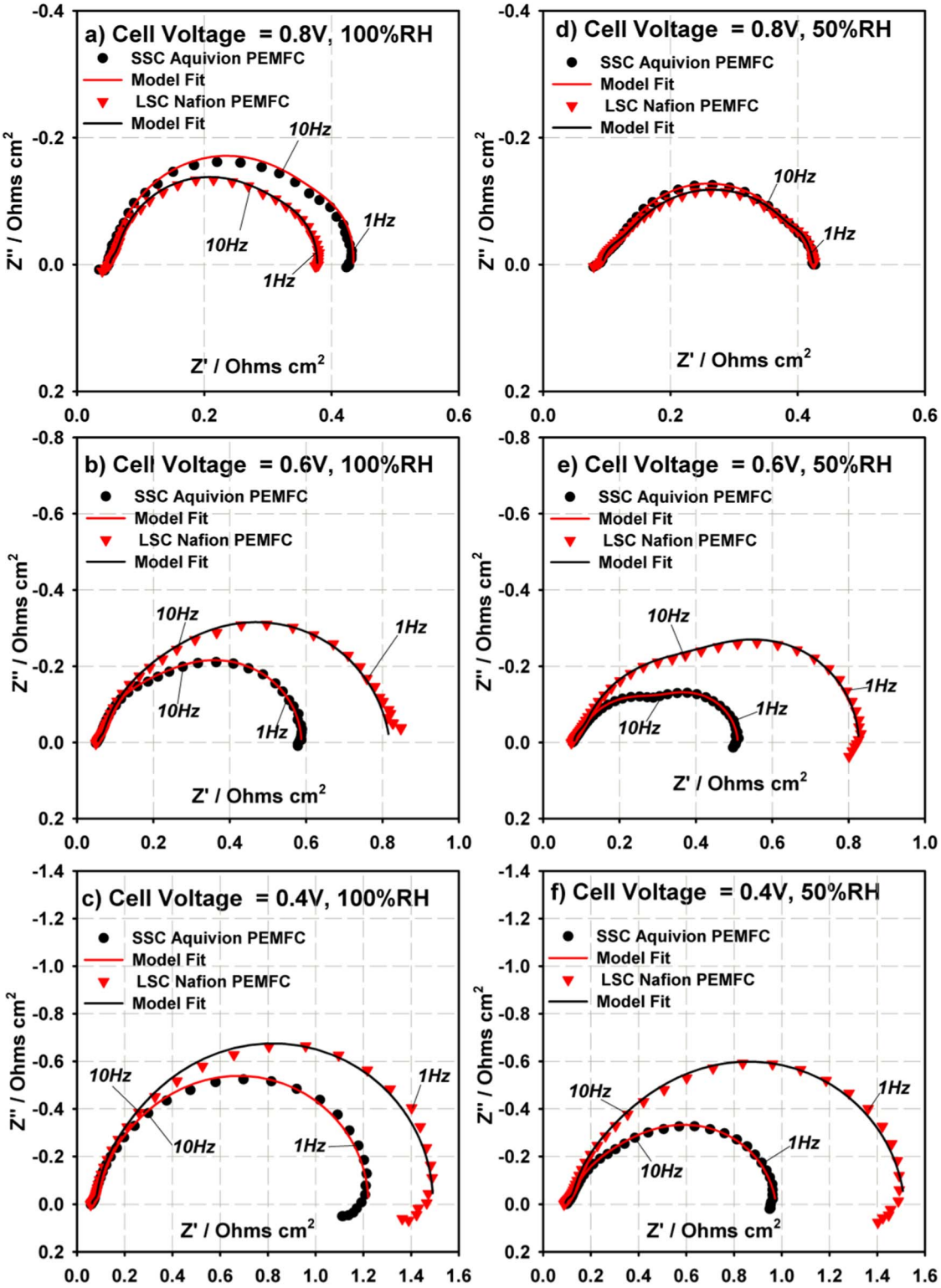

Figure 10. In situ EIS obtained at cell temperature of 80°C, ambient pressure, 100% RH when the cell is operated at a) 0.80 V, b) 0.60 V and c) 0.40 V. In situ electrochemical impedance spectra obtained at cell temperature of 80°C, ambient pressure, 50% RH when the cell is operated at d) 0.80 V, e) 0.60 V and f) 0.40 V.

and microstructure. The SSC Aquivion ionomer has a higher ion exchange capacity; applying this ionomer in the cathode CL reduces the cathode H^+ transport resistance by 61% compared to LSC Nafion. Additionally, we reconcile the improved performance based on the ~30% reduction in total O_2 transport resistance in the PEMFCs with SSC Aquivion in the cathode CL, which we ascribe to the ~2x higher micropore content of the cathode CLs with the SSC Aquivion vs. LSC Nafion ionomers. Such micropores have been modeled to be critical in water management, as they can improve water evaporation to the gas phase, and improve heat transfer. Therefore as the water production of the fuel cell increases, the role of the micropores becomes more important.

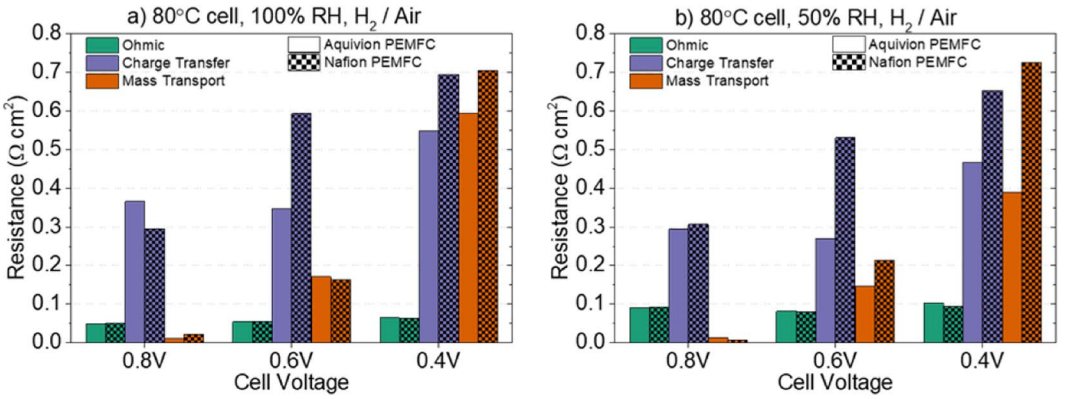

Figure 11. Comparison of the sources of resistance obtained by the ECM fitting from the EIS spectra recorded and presented in Figure 10 at cell temperature of 80°C, in ambient pressure H_2/Air at a) 100% RH and b) 50% RH.

While many have also attributed the increased performance imparted through the use of SSC ionomers to more uniform ionomer distributions, and thus less O_2 resistance, we can qualitatively explain our results on the basis of lower cathode H^+ transport resistance in combination with higher microporosity leading to improved proton conduction and less local flooding with water.

Our work still leaves open many questions about how using SSC ionomers improves fuel cell performance. We cannot rule out from our studies the chemical role of SSC ionomers and how this affects interaction with the Pt particles, hydrophobicity/hydrophilicity, and water management. We also have not probed the long-term durability of the CLs containing the SSC Aquivion ionomers. Another question remains in determining whether the distribution of the LSC Nafion ionomers might be improved with more attention to the ink formulation, and perhaps by employing a fabrication method other than ultrasonic spray. However, we can conclude that under the conditions tested herein, the use of the SSC ionomer contributes significantly to the improved performance of PEMFCs. Follow-on modeling work will be attempted to further confirm this explanation.

Acknowledgments

The authors are grateful to the Office of Naval Research for financial support of this project. RWA is a postdoctoral fellow supported by the American Society for Engineering Education. RMEH is a postdoctoral fellow supported by the National Research Council.

ORCID

Yannick Garsany https://orcid.org/0000-0002-8943-7174
Robert W. Atkinson III https://orcid.org/0000-0001-7575-0584
Benjamin D. Gould https://orcid.org/0000-0001-5822-4160

References

1. S. Litster and G. McLean, *J. Power Sources*, **130**, 61 (2004).
2. J. P. Owejan, J. E. Owejan, and W. B. Gu, *J. Electrochem. Soc.*, **160**, F824 (2013).
3. T. Tanuma and S. Kinoshita, *J. Electrochem. Soc.*, **161**, F94 (2014).
4. S. M. Kim, C.-Y. Ahn, Y.-H. Cho, S. Kim, W. Hwang, S. Jang, S. Shin, G. Lee, Y.-E. Sung, and M. Choi, *Sci. Rep.*, **6**, 26503 (2016).
5. M. Eikerling, *J. Electrochem. Soc.*, **153**, E58 (2006).
6. Q. Wang, M. Eikerling, D. Song, and Z. Liu, *J. Electroanal. Chem.*, **573**, 61 (2004).
7. M. Uchida, Y. C. Park, K. Kakinuma, H. Yano, D. A. Tryk, T. Kamino, H. Uchida, and M. Watanabe, *PCCP*, **15**, 11236 (2013).
8. M. Lee, M. Uchida, H. Yano, D. A. Tryk, H. Uchida, and M. Watanabe, *Electrochim. Acta*, **55**, 8504 (2010).
9. T. E. Springer, T. A. Zawodzinski, M. S. Wilson, and S. Gottesfeld, *J. Electrochem. Soc.*, **143**, 587 (1996).
10. A. Ghielmi, P. Vaccarono, C. Troglia, and V. Arcella, *J. Power Sources*, **145**, 108 (2005).
11. E. Moukheiber, G. De Moor, L. Flandin, and C. Bas, *J. Membr. Sci.*, **389**, 294 (2012).
12. N. N. Zhao, D. Edwards, C. Lei, K. P. Wang, J. Li, Y. M. Zhang, S. Holdcroft, and Z. Q. Shi, *J. Power Sources*, **242**, 877 (2013).
13. M. Yandrasits, M. Lindell, M. Schaberg, and M. Kurkowski, *Electrochem. Soc. Interface*, **26**, 49 (2017).
14. C. Lei, D. Bessarabov, S. Y. Ye, Z. Xie, S. Holdcroft, and T. Navessin, *J. Power Sources*, **196**, 6168 (2011).
15. J. Peron, D. Edwards, M. Haldane, X. Y. Luo, Y. M. Zhang, S. Holdcroft, and Z. Q. Shi, *J. Power Sources*, **196**, 179 (2011).
16. Y. C. Park, K. Kakinuma, H. Uchida, M. Watanabe, and M. Uchida, *J. Power Sources*, **275**, 384 (2015).
17. M. J. Choo, K. H. Oh, J. K. Park, and H. T. Kim, *Chemelectrochem*, **2**, 382 (2015).
18. Y. C. Park, H. Tokiwa, K. Kakinuma, M. Watanabe, and M. Uchida, *J. Power Sources*, **315**, 179 (2016).
19. M. Breitwieser, T. Bayer, A. Büchler, R. Zengerle, S. M. Lyth, and S. Thiele, *J. Power Sources*, **351**, 145 (2017).
20. L. G. A. Melo, A. P. Hitchcock, J. Jankovic, J. Stumper, D. Susac, and V. Berejnov, *ECS Trans*, **80**, 275 (2017).
21. M. B. Sassin, Y. Garsany, B. D. Gould, and K. E. Swider-Lyons, *Anal. Chem.*, **89**, 511 (2017).
22. M. B. Sassin, Y. Garsany, B. D. Gould, and K. Swider-Lyons, *J. Electrochem. Soc.*, **163**, F808 (2016).
23. R. W. Atkinson III, Y. Garsany, B. D. Gould, K. E. Swider-Lyons, and I. V. Zenyuk, *ACS Appl. Energy Mater.*, **1**(1), 191 (2018).
24. J. B. Ge, A. Higier, and H. T. Liu, *J. Power Sources*, **159**, 922 (2006).
25. C. Simon, F. Hasché, and H. A. Gasteiger, *J. Electrochem. Soc.*, **164**, F591 (2017).
26. H. A. Gasteiger, S. S. Kocha, B. Sompalli, and F. T. Wagner, *Appl Catal B-Environ*, **56**, 9 (2005).
27. K. R. Cooper, V. Ramani, J. M. Fenton, and H. R. Kunz, *Experimental Methods and Data Analyses for Polymer Electrolyte Fuel Cells*, Scribner Associates, Incorporated (2007).
28. Y. Zhai, K. Bethune, G. Bender, and R. Rocheleau, *J. Electrochem. Soc.*, **159**, B524 (2012).
29. D. R. Baker, D. A. Caulk, K. C. Neyerlin, and M. W. Murphy, *J. Electrochem. Soc.*, **156**, B991 (2009).
30. J. A. Xie, F. Xu, D. L. Wood, K. L. More, T. A. Zawodzinski, and W. H. Smith, *Electrochim. Acta*, **55**, 7404 (2010).
31. T. Suzuki, S. Tsushima, and S. Hirai, *Int. J. Hydrogen Energy*, **36**, 12361 (2011).
32. H. R. Yu, J. M. Roller, W. E. Mustain, and R. Maric, *J. Power Sources*, **283**, 84 (2015).
33. A. Parthasarathy, S. Srinivasan, A. J. Appleby, and C. R. Martin, *J. Electrochem. Soc.*, **139**, 2530 (1992).
34. A. Orfanidi, P. Madkikar, H. A. El-Sayed, G. S. Harzer, T. Kratky, and H. A. Gasteiger, *J. Electrochem. Soc.*, **164**, F418 (2017).
35. K. O'Neil, J. P. Meyers, R. M. Darling, and M. L. Perry, *Int. J. Hydrogen Energy*, **37**, 373 (2012).
36. A. Ohma, T. Mashio, K. Sato, H. Iden, Y. Ono, K. Sakai, K. Akizuki, S. Takaichi, and K. Shinohara, *Electrochim. Acta*, **56**, 10832 (2011).
37. Y. H. Tang, J. J. Zhang, C. J. Song, H. Liu, J. L. Zhang, H. J. Wang, S. Mackinnon, T. Peckham, J. Li, S. McDermid, and P. Kozak, *J. Electrochem. Soc.*, **153**, A2036 (2006).